Applied Surface Science 376 (2016) 97–104

Contents lists available at ScienceDirect

Applied Surface Science

journal homepage: www.elsevier.com/locate/apsusc

Investigation of fluorine adsorption on nitrogen doped $MgAl_2O_4$ surface by first-principles

Xiaojun Lv[a], Zhenming Xu[a], Jie Li[a,*], Jiangan Chen[b], Qingsheng Liu[c]

[a] School of Metallurgy and Environment, Central South University, Changsha 410083, China
[b] Faculty of Resource and Environmental Engineering, Jiangxi University of Science and Technology, Ganzhou 341000, China
[c] Faculty of Metallurgical and Chemical Engineering, Jiangxi University of Science and Technology, Ganzhou 341000, China

ARTICLE INFO

Article history:
Received 5 February 2016
Received in revised form 9 March 2016
Accepted 15 March 2016
Available online 16 March 2016

Keywords:
Density functional theory
N doping
Fluorine adsorption

ABSTRACT

The nature of fluorine adsorption on pure and N doped $MgAl_2O_4$ surface has been investigated by first-principles calculations based on the density functional theory. Calculated results indicate that $MgAl_2O_4$ surface is fluorine-loving, not hydrophilic. Nitrogen doped $MgAl_2O_4$ (100) surface shows the highest fluorine adsorption performance and fluorine atom preferentially adsorbs on the Mg-Al bridge site. The fluorine adsorption intensity follow this order: Nitrogen doped $MgAl_2O_4$ (100) > Al_2O_3 (0001) > $MgAl_2O_4$ (100) > MgO (100). In-depth PDOS analysis suggested that 2*p* orbitals of F atom strongly hybridized with 3*s*- and 3*p*-orbitals of Al atom contribute to its high adsorption intensity. According to the analysis of Hirshfeld charge, the excellent fluorine adsorption performance of nitrogen doped $MgAl_2O_4$ attributes to the electron compensation effect of nitrogen atom and strong electrostatic interactions. All these evidences demonstrate a fact nitrogen doped $MgAl_2O_4$ is a promising candidate for fluorine removal.

1. Introduction

Fluorine, the most electronegative and reactive element, existing in the form of fluorinion in drinking water is currently of great concern because of its significant influence on public health [1–4]. In the reports of WHO [1,5–7], fluorine is regarded as one of the contaminants in water and the maximum fluorine contamination limit of 1.0 mg/L in drinking water may lead to some disease, such as dental fluorosis and skeletal fluorosis. Hence, controlling the level of fluorine in the source water is crucial to protecting public health. Many techniques have been applied for the removal of fluorine using chemical precipitation or physical treatment, such as precipitation [8,9], adsorption [10,11], ion exchange [12,13], and electrodialysis [14]. Among them, adsorption process is the most promising one due to its high efficiency, easy operation and maintenance, lower cost and more environment friendly process [10,11]. So far, alumina and its derivative adsorbents have been used to reduce the fluorine level of aqueous system [6,15–19]. To further search for adsorbent with higher adsorption capacity, amounts of other efforts have been made. Magnesia and its corresponding composite materials, such as magnesia-amended activated alumina granules [17], magnesium-doped nano-ferrihydrite [10,20], magnesium-incorporated bentonite clay [21], and magnesia-amended silicon dioxide [22], etc. have been successfully synthesized and applied for fluorine removal.

It is worth noting that another important compound magnesium aluminum spinel has been widely used as the functional materials for heterogeneous catalysts, humidity sensors, and ultrafiltration membranes due to its stable and stable surface properties [23,24]. However, to the best of authors' knowledge, to date, no experimental research on magnesium aluminum spinel for fluorine removal has been reported, so we should explore whether spinel $MgAl_2O_4$ material is appropriate for fluorine removal or not. Before carrying out experimental work, we have firstly performed thorough literature survey about the microscopic adsorption mechanism of fluorine on $MgAl_2O_4$ surface, indicating no theoretical investigation has been carried out up to now. While some other published works have a certain reference significance for our work, such as the stability and electronic structure of $MgAl_2O_4$ (111) surfaces [25], surface energy of spinel $MgAl_2O_4$ [23], dissociative adsorption of water on the surfaces of spinel $MgAl_2O_4$ [24], and hydrogen fluoride adsorption and reaction on the α-Al_2O_3 (0001) surface [26]. Computer simulation based on the density-functional theory (DFT) has been proven to be a cost-effective, powerful and reliable tool to discern adsorption at the atom level [27–32]. Therefore, a detailed theoretical investigation of fluorine adsorption on the surface of $MgAl_2O_4$ and its derivative compound is necessary.

* Corresponding author.
E-mail address: 15216105346@163.com (J. Li).

http://dx.doi.org/10.1016/j.apsusc.2016.03.108
0169-4332/

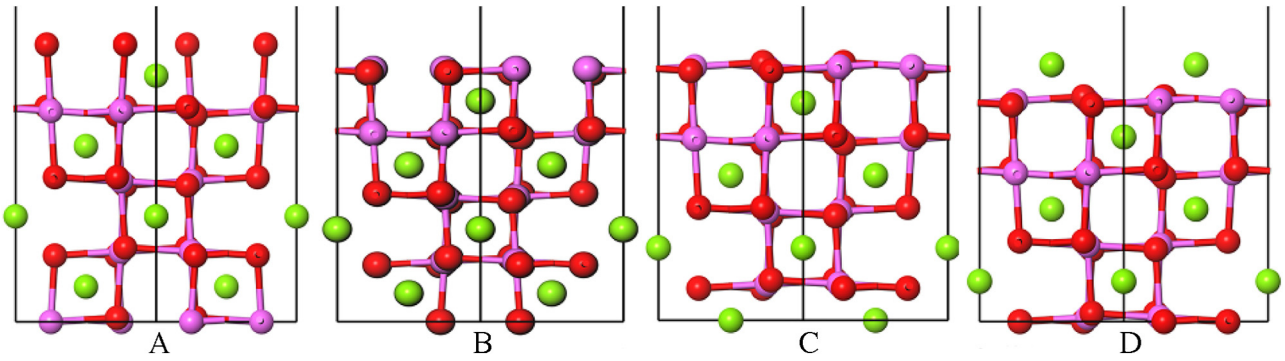

Fig. 1. Side views of four different $p(1 \times 1)$ slab models of $MgAl_2O_4$ (100) surface. The red, pink and green spheres represent the O, Al, and Mg atom, respectively. (For interpretation of the references to colour in this figure legend, the reader is referred to the web version of this article.)

Aiming to discern the detailed adsorption mechanism, first-principles calculations based on the density functional theory (DFT) and the periodic slab models were employed to explore the nature of fluorine adsorption on $MgAl_2O_4$ surface. Various important properties such as adsorption geometry structure, adsorption energy, Milliken population, and density of states (DOS) were analyzed and compared to the calculated results of MgO and Al_2O_3. Moreover, its derivative compound nitrogen doped $MgAl_2O_4$ was also calculated and discussed for expecting enhanced adsorption performance.

2. Computational methodology and models

All calculations were performed using the density functional theory (DFT) with the exchange-correlation functional treated in the spin-polarized GGA-PBE [33] as implemented in CASTEP package [34]. The ultrasoft pseudo potentials (USPP) introduced by Vanderbilt [35] have been employed for all ion-electron interactions. Convergence with respect to both energy cutoff and *k*-point mesh has been tested. As a result of convergence, an energy cutoff of 400 eV was chosen to ensure that the total energies were converged within 1×10^{-6} eV/atom. For the Brillouin zone sampling, we carried out $4 \times 4 \times 4$ *k*-points mesh for $MgAl_2O_4$ bulk using the method of Monkhorst-Pack [36]. To prepare the most-stable configuration for following surface energy calculations, full optimization of the fractional coordinates and the lattice parameters was performed by means of total energy minimization [37]. All atoms were relaxed to their equilibrium positions when the total energy change was finally converged to 10^{-5} eV/atom, the force on each atom was converged to 0.03 eV/Å, the stress on each atom was converged to 0.05 GPa, and displacement changes of each atom was converged to 0.001 Å.

Tests of vacuum region of different thickness show that adding a 18 Å vacuum region on the chapped surface is good enough to fairly represent the bulk material. Surface energy calculations reported here were performed using the $p(1 \times 1)$ slab structures, where the periodicity was still held in the directions parallel to surface atoms. In all surface calculations, the use of symmetry in bulk crystal was failed and *k*-point mesh was cut down to a single *k*-point in the direction perpendicular to surface planes, while the *k* grid in the directions parallel to surface atoms was used as the bulk calculations [38]. According to the test results of energy vs. the height of surface layers [39] and to maintain the stoichiometry of surface slabs as the bulk crystal, when the intercept depth is a, $\sqrt{2}a$ and $\sqrt{3}a$ Å ($a = 8.06$ [40], is equal to the lattice parameter of $MgAl_2O_4$) for (100), (110) and (111) surfaces with a total number of 4, 8, 6 $MgAl_2O_4$ formula units, respectively, the change of energy is negligibly small. Therefore, a slab of a, $\sqrt{2}a$ and $\sqrt{3}a$ Å with a relaxation layer of 5.0, 5.0 and 3.47 Å is enough to obtain a converged surface energy in view of the computational precision and efficiency. In this work, slab calculations for the (100) and (110) surfaces were carried out with the outer four atomic layers allowed to move, while the remaining internal layers were frozen at bulk positions to simulate the bulk of this material. In addition, all slab calculations for the (111) surfaces were conducted with the outer six atomic layers permitted to relax, whereas the rest of internal atomic layers were restrained. For fluorine adsorption calculations, the $p(1 \times 1)$

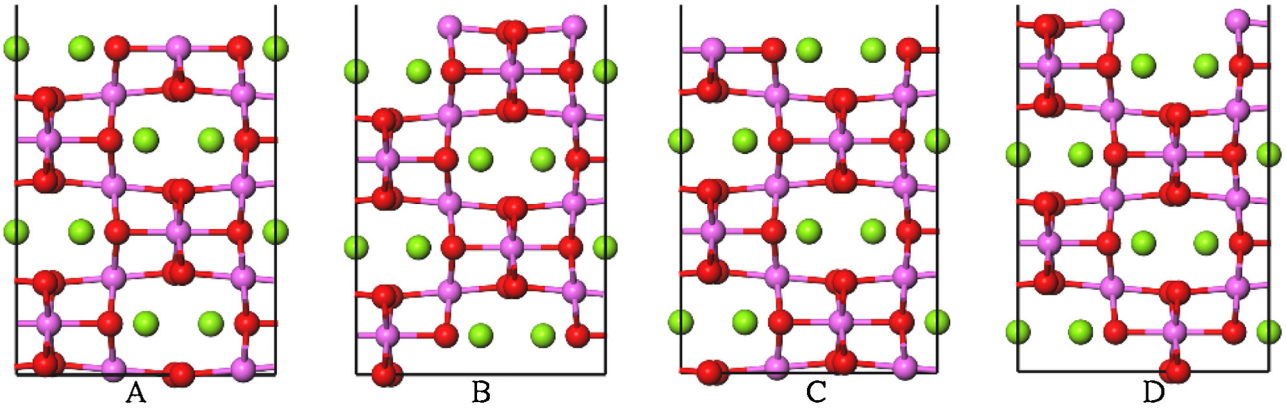

Fig. 2. Side views of four different $p(1 \times 1)$ slab models of $MgAl_2O_4$ (110) surface. The red, pink and green spheres represent the O, Al, and Mg atom, respectively. (For interpretation of the references to colour in this figure legend, the reader is referred to the web version of this article.)

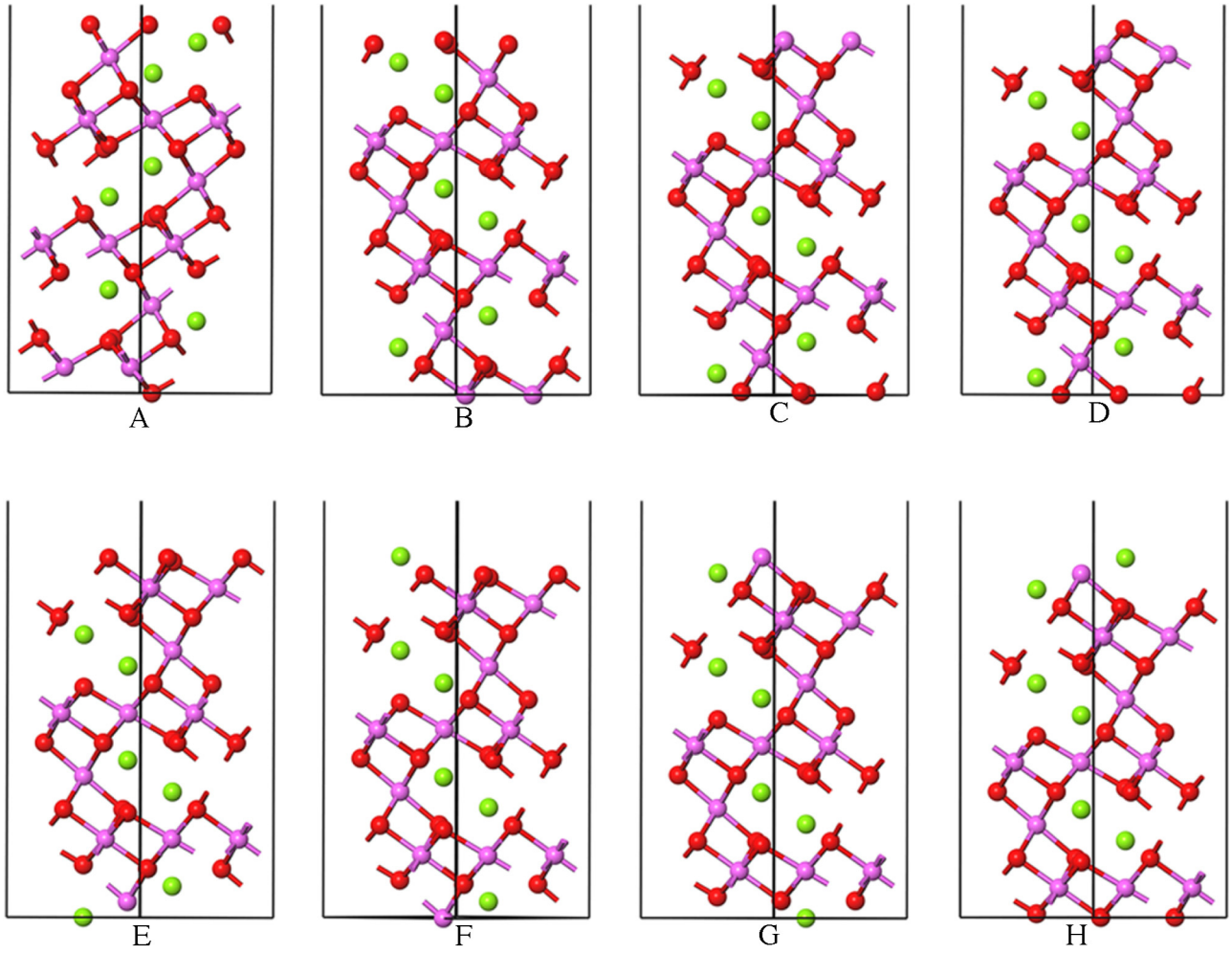

Fig. 3. Side views of eight different $p(1 \times 1)$ slab models of $MgAl_2O_4$ (111) surface. The red, pink and green spheres represent the O, Al, and Mg atom, respectively. (For interpretation of the references to colour in this figure legend, the reader is referred to the web version of this article.)

units were adopted to simulate the high concentration adsorbate on $MgAl_2O_4$ surface, therefore, (100) surfaces were 5.66×5.66 Å^2 with a k-point mesh of $6 \times 6 \times 1$. The (110) surface supercells were 8.0×5.66 Å^2 with a k-point mesh of $4 \times 6 \times 1$. In addition, all the (111) surfaces were $0.5\sqrt{3} \times 11.32 \times 11.32$ Å^2 with X, Y axes forming a 60° angle employing a $4 \times 4 \times 1$ k-point mesh.

The surface energy is composed of corresponding cleavage and relaxation energy [25]. Cleaving one crystal, two terminated surfaces with the equally slab unrelaxed energy are created simultaneously, e.g. slab model A and B, C and D in Fig. 1. Therefore, the cleavage energies E_C can be obtained from the total energy of unrelaxed slab through the following equation: $E_C = (E_{slab}^{unrel}(A) + E_{slab}^{unrel}(B) - xE_{Bulk})/2S$, where $E_{slab}^{unrel}(A)$ and $E_{slab}^{unrel}(B)$ is the energy of unrelaxed slab (A) and its complementary slab (B), respectively [41,42]. E_{Bulk} is the energy per formula unit, x is the total number of formula unit in two slabs, 2 means the two surfaces created by the cleavage and S is the corresponding surface area. Next, the surface relaxation energy is calculated according to: $E_R = (E_{slab}^{rel} - E_{slab}^{unrel})/2S$, here, E_{slab}^{rel} is the energy of a slab after structure relaxation [25]. Finally, the surface energy is obtained as a sum of the cleavage and relaxation energy: $E_{surf} = E_C + E_R$. The adsorption energy was calculated according to the following equation: $E_{ad} = E(\text{F-slab}) - [E(\text{F}) + E(\text{slab})]$, here, E(F-slab) is the total energy of the adsorbate-substrate system, E(slab) and E(F) is the energy of the substrate and F atom, respectively. Usually, E_{ad} is negative for an exothermic adsorption. The more negative the adsorption energy, the stronger adsorption of fluorine atom on $MgAl_2O_4$ surface.

3. Results and discussion

3.1. Surface stability of $MgAl_2O_4$

Before studying the fluorine adsorption, we have firstly investigated the surface properties of adsorption substrate $MgAl_2O_4$, because adsorption process usually occurs on the most-stable cleaving surface [43]. The stability of surface system varies depending on the exposed atoms. Therefore, combining with the symmetry of spinel $MgAl_2O_4$ crystal, three main crystal planes of (100), (110) and (111) and different atoms exposing on the outer surface was considered for the calculated models. For example, along the [111] direction in $MgAl_2O_4$ crystal, the atomic stacking sequence is found as -O-Al-O-Mg-Al-Mg-O-. Correspondingly, surface can be divided into three types: Al-terminated, Mg-terminated and O-terminated. Among them, there are two different cases of Al-terminated surface: one is the second layer composed of Mg atoms, and the other is the second layer composed of O atoms, which is defined as Al(O)-termination and Al(Mg)-termination, respectively (Fig. 3(c) and (g)). Similarly, Mg-terminated surface also has two cases of

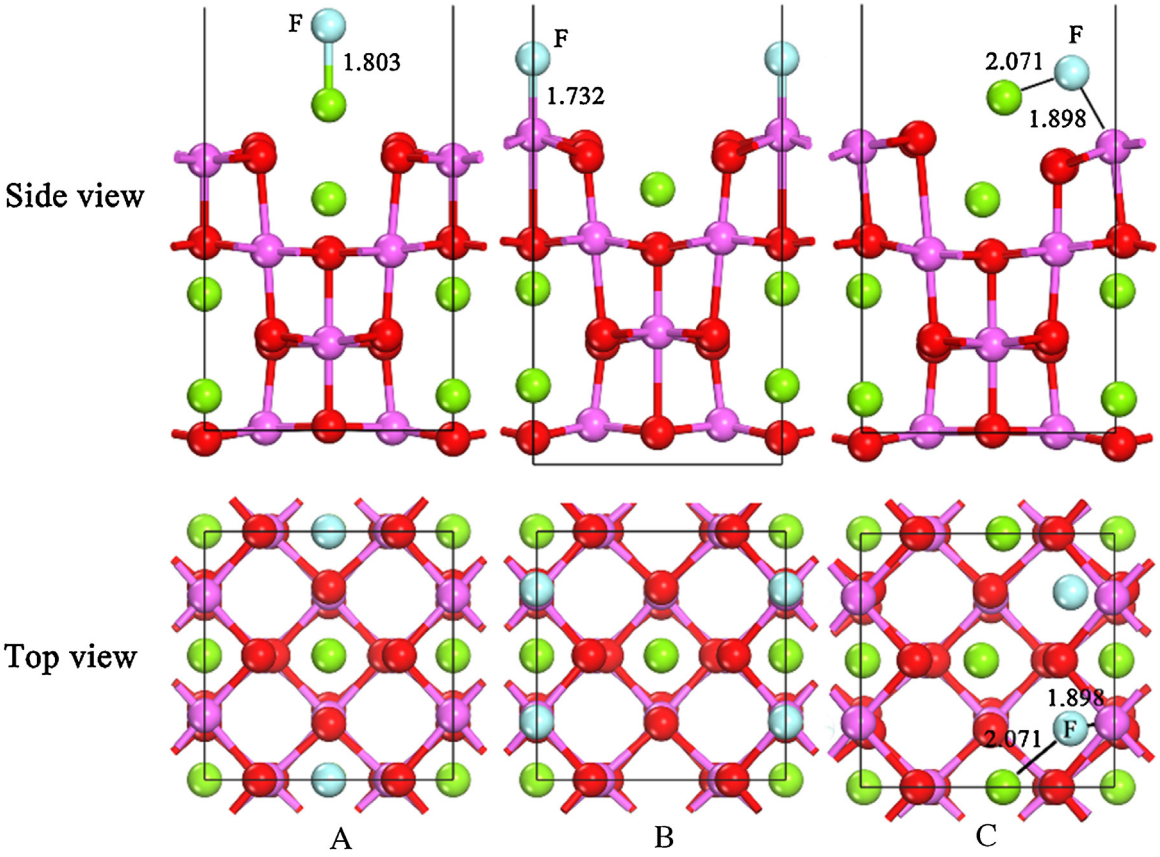

Fig. 4. Adsorption configuration of fluorine adsorption on $MgAl_2O_4$ (100) surface. (A) Mg-top site; (B) Al-top site; and (C) Mg-Al-bridge site. The red, pink, green and blue spheres represent the O, Al, Mg and F atom, respectively. (For interpretation of the references to colour in this figure legend, the reader is referred to the web version of this article.)

Mg(Al)-termination and Mg(O)-termination (Fig. 3(f) and (h)). For O-terminated $MgAl_2O_4$ (111) surface, there are four O atom positions with a small difference. If the top two layers are composed of O atom layers while the third layer consist of Mg or Al, it is correspondingly defined as O_2(Mg)-termination or O2(Al)-termination (Fig. 3(b) and (e)). If the top layer consist of O atom layer while the second layer is Mg or Al atoms, it is correspondingly defined as O(Mg)-termination or O(Al)-termination (Fig. 3(a) and (d)). Considering different types and sites of atom exposed to vacuum, a total of A-H eight symmetrical and stoichiometric surface models of $MgAl_2O_4$(111) are shown in Fig. 3(a-h). Moreover, being similar to above definition of (111), four slab models were obtained for the (100) and (110) surface, as shown in Figs. 1 (a–d) and 2 (a–d), respectively. Some structure information such as atom exposed and clipping planes is listed in Table 1. For example in Table 1, when the (100) surface is cut through the plane (0.25, 0, 0), only Mg atom will be exposed at outer surface. When the (100) surface is cut through plane (0.125, 0, 0), Al and O atom will be exposed at outer surface.

Calculated results of cleavage, relaxation and surface energies of multiple terminations for $MgAl_2O_4$ (100), (110) and (111) surfaces are listed in Table 1. It can be seen that different terminations and plane directions result in large difference in surface energy. While in the identical orientation surface, there is a pair of surface structure having the same cleavage, relaxation and surface energy, such as (100) A and (100) B. It is because of the complementation and same number of broken bonds generated by cleaving one $MgAl_2O_4$ bulk. Strong surface relaxations were found in the (100) orientation, but only moderate surface relaxations were found in the (110) and (111) surface. The surface energy of (100) A and B is same 4.24 J/m^2 and larger than (100) C and D of 2.317 J/m^2. Among all calculated surfaces, (100) C and D exposing Al-O2, Mg atoms created by the clipping plane (0.139,0,0) and (0.25,0,0) have the lowest cleavage and surface energy, and it is in good agreement with 2.27 J/m^2 by G.de With [23]. When the (110) surfaces expose Al and O atoms, the surface energies of them are from 2.679 to 3.824 J/m^2 and slightly higher than (100) C and D. When the (110) surfaces expose Mg, Al and O atoms, the surface energy will drop to 2.679 J/m^2. As for (111) surface, our calculated surface energies are close to that in the

Table 1
Calculated cleavage, relaxation and surface energies (J/m^2) for multiple terminations of $MgAl_2O_4$ surfaces.

Surface	Atom exposed	Clipping plane	E_C (J/m^2)	E_R (J/m^2)	E_S(J/m^2)	Ref
(100) A	O	(0.111,0,0)	5.263	−1.025	4.238	
B	Al-O	(0.125,0,0)	5.263	−1.025	4.238	
C	Al-O2	(0.139,0,0)	2.818	−0.501	2.317	2.27[a]
D	Mg	(0.25,0,0)	2.818	−0.501	2.317	
(110) A	Mg-Al-O	(0.25,0.25,0)	3.326	−0.647	2.679	
B	Al-O	(0.5,0.5,0)	4.153	−0.329	3.824	
C	Mg-Al-O	(0.75,0.75,0)	3.326	−0.647	2.679	2.85[a]
D	Al-O	(1,1,0)	4.153	−0.329	3.824	
(111) A	O(Mg)	(0.139,0.139,0.139)	5.168	−0.405	4.763	5.438[b]
B	O2(Mg)	(0.168,0.168,0.168)	7.132	−0.335	6.797	7.538[b]
C	Al(O)	(0.375,0.375,0.375)	7.132	−0.335	6.797	7.786[b]
D	O(Al)	(0.582,0.582,0.582)	5.168	−0.405	4.763	5.248[b]
E	O2(Al)	(0.611,0.611,0.611)	5.642	−0.283	5.359	5.641[b]
F	Mg(Al)	(0.75,0.75,0.75)	3.536	−0.310	3.226	3.428[b]
G	Al(Mg)	(0.875,0.875,0.875)	3.536	−0.310	3.226	3.481[b]
H	Mg(O)	(1,1,1)	5.642	−0.283	5.359	5.925[b]

[a] Reference [23].
[b] Reference [25].

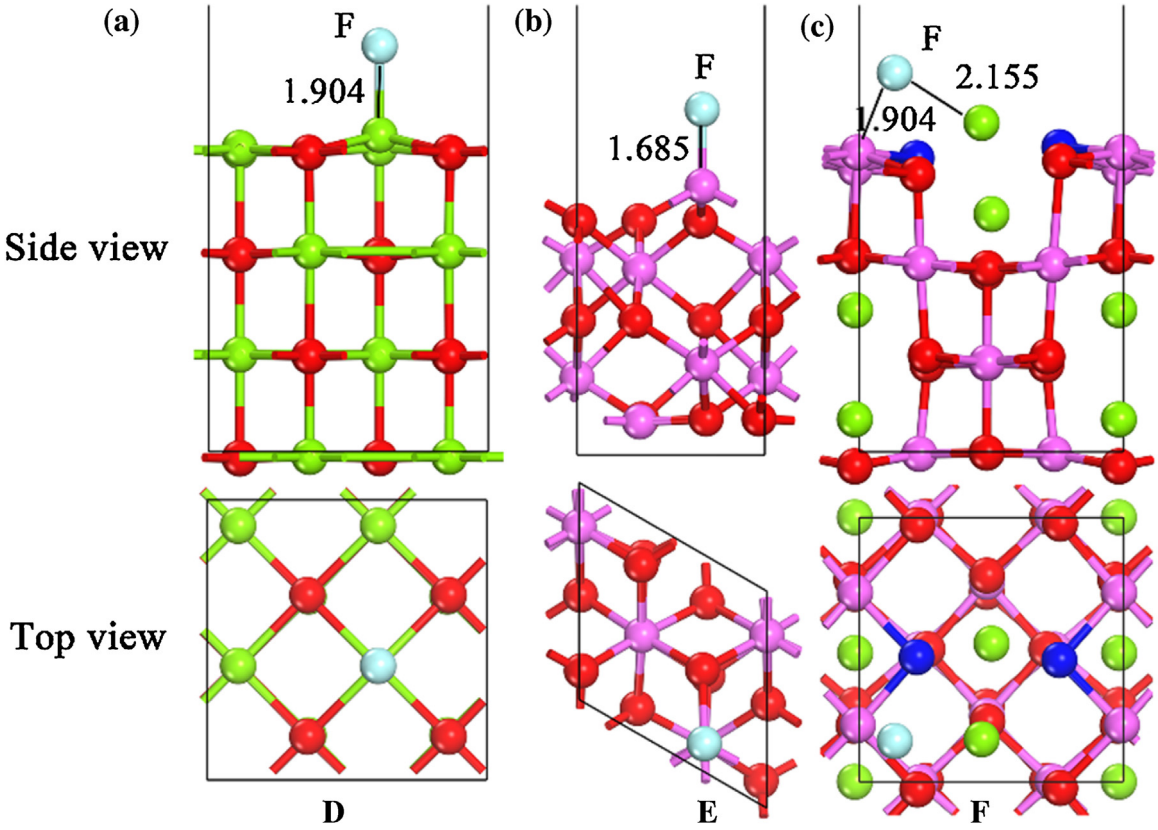

Fig. 5. Adsorption configuration of fluorine adsorption on (a) MgO (100), (b) Al_2O_3 (0001) and (c) nitrogen doped $MgAl_2O_4$ (100) surface. The red, pink, green, blue and cyan spheres represent the O, Al, Mg, F and N atom, respectively. (For interpretation of the references to colour in this figure legend, the reader is referred to the web version of this article.)

previous work [25], but are slightly smaller than that. In addition, the (111) B and C have the largest cleavage energy of 7.132 J/m^2 and surface energy of 6.797 J/m^2 due to that much energy is need to break the strong covalent Al-O bonds of (111) C surface with only Al atoms exposed. Therefore, we can conclude that (111) is the highest energy surface, which is consistent with the published reports [23,41]. On the contrary, the low-index (100) C and D surface is the most stable and dominant. These results indicate that, $MgAl_2O_4$ (100) surface terminated with Al-O2 or Mg atoms is most likely to be exposed to real environment. Therefore, the following fluorine adsorption was performed on this most-stable surface (100) C and D.

3.2. Fluorine adsorption on $MgAl_2O_4$ (100) surface

A single adatom was initially put above different sites of $MgAl_2O_4$ (100) surface and then full optimizations of the fractional coordinates for the absorption periodic model were carried out. The optimized configurations of fluorine adsorption are depicted in Fig. 4. The adsorption energies, geometric structure parameters and Hirshfeld charge for fluorine adsorption on $MgAl_2O_4$ (100) surface are listed in Table 2. Calculated adsorption energies indicate that the stability of fluorine adsorption follow the order of Mg-Al bridge site (case C) > Al-top site (case B) > Mg-top site (case A) with adsorption energies within −0.92 to −5.02 eV on $p(1 \times 1)$ $MgAl_2O_4$ (100) surface, demonstrating that fluorine chemically adsorbs on all sites of $MgAl_2O_4$ (100) surface. In addition, in order to understand the tendency of atomic charge transfer between the adatom and substrate, Hirshfeld population analysis was carried out. Viewed from Table 2, the adsorbed fluorine atoms are all negatively charged in the three stable configurations within −0.173 to −0.378e, indicating that electrons transfer from $MgAl_2O_4$ substrate to F adatom. Because relatively more electrons transfer from Mg-Al bridge (case C) than Mg (case A) to adatom F, Fluorine adsorbs on $MgAl_2O_4$ (100) surface with the strongest electrostatic interactions. Therefore, F atom preferentially adsorbs on the Mg-Al bridge sites of $MgAl_2O_4$ (100) surface, which is in agreement with above stability orders. Moreover, considering the fluorine adsorption and removal usually occurs in the aqueous system, we have reason to doubt that whether water may affect the fluorine adsorption behavior on $MgAl_2O_4$ surface or not? Hence, water molecule adsorption on $MgAl_2O_4$ (100) surface was also investigated. The calculated adsorption energy of single water molecule is a positive value of 3.74 eV and in agreement with the molecular dynamics calculated values of 1.66–2.62 eV by G. de With [24], indicating $MgAl_2O_4$ surface is not hydrophilic. We can conclude that water molecules have negligible influence on the fluorine adsorption behavior, and our fluorine adsorption model without considering water molecules is reasonable.

Compared to the clean $MgAl_2O_4$ (100) surface (Fig. 1), it is especially obvious that the surface atoms of optimized adsorption configuration have deviated from their initial coordinates in clean surface unit. Moreover, the atoms of adsorption site in the substrate are consistently pulled to the direction away from the surface plane. This is due to the charge redistribution of surface atoms after F adatom being introduced. The distortion degree of fluorine adsorption on $MgAl_2O_4$ (100) surface follows the order of C > B > A, which is consistent with the order of fluorine adsorption stability. It is also worth pointing out that the atom rearrangement of $MgAl_2O_4$ (100) surface with absorbed F atoms is the process of energy release, not seriously destroying $MgAl_2O_4$ surface. In addition, fluorine adsorption on the Mg top site of MgO (100) and Al top site of Al_2O_3(0001)

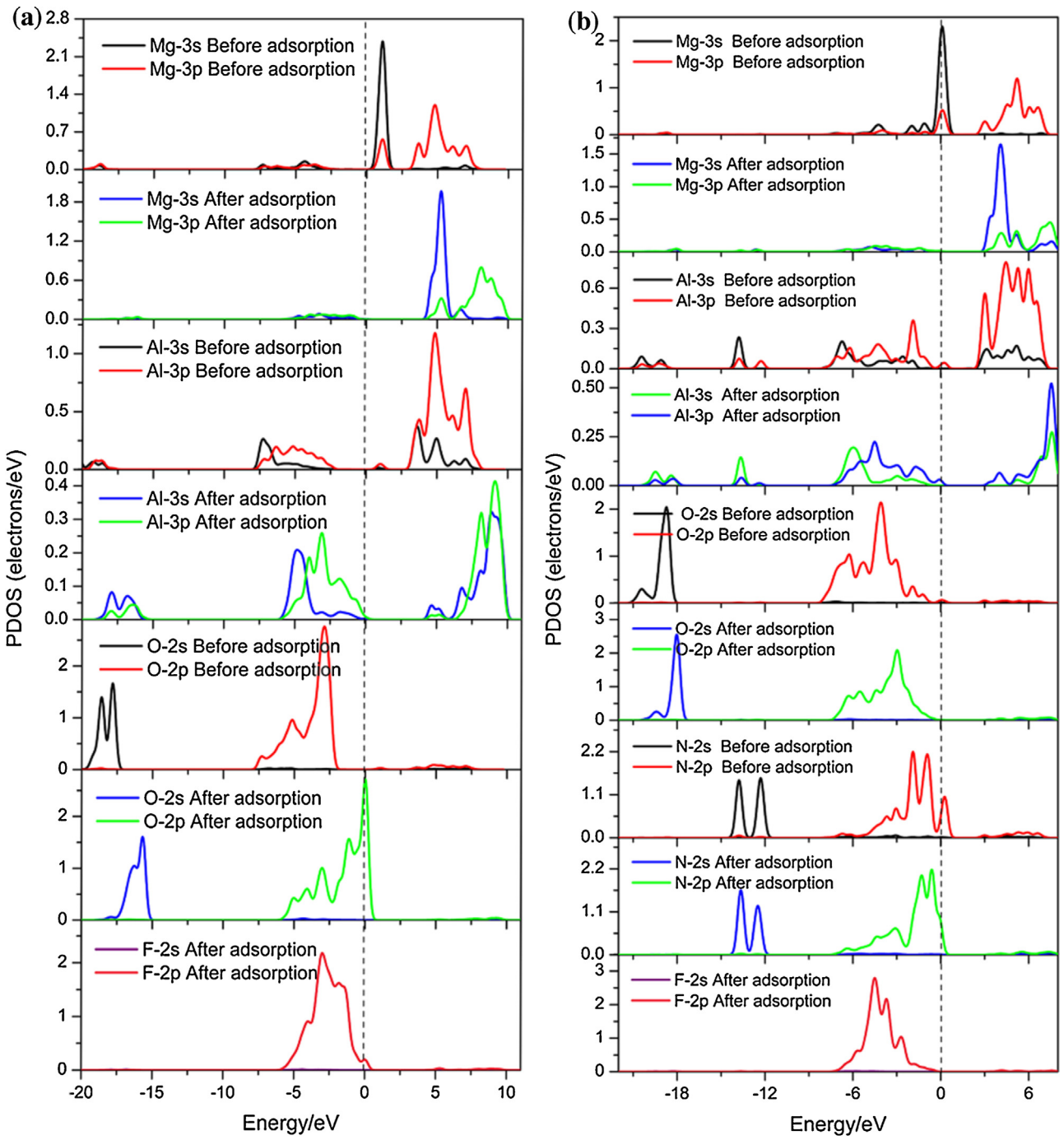

Fig. 6. PDOS for surface system before and after fluorine adsorption on (a) pure and (b) nitrogen doped $MgAl_2O_4$ (100) surface. The Fermi level is set to be zero (dashed line in figures).

Table 2
Adsorption energies (E_{ads} in eV), geometric structure parameters (D_{X-Y} denotes bond distance between adsorbed F and Mg, Al atom, in Å) and Hirshfeld charges of the outermost atoms (negative value means electrons acquisition, in *e*) for fluorine adsorption on pure and N doped $MgAl_2O_4$ (100) surface in comparison with calculated results of MgO and Al_2O_3.

	Case	E_{ads}	D_{F-Mg}	D_{F-Al}	Q_F	Q_{Mg}	Q_{Al}
$MgAl_2O_4$ (100)	A(Mg top site)	−0.92	1.803		−0.378	0.623	
	B(Al top site)	−2.301		1.732	−0.173		0.435
	C(Mg-Al bridge site)	−5.016	2.071	1.898	−0.241	0.697	0.406
MgO (100)	D(Mg top site)	−4.502	1.904		−0.387	0.416	
Al_2O_3 (0001)	E(Al top site)	−5.341		1.685	−0.226		0.556
N doped $MgAl_2O_4$ (100)	F(Mg-Al bridge site)	−5.592	2.155	1.904	−0.266	0.613	0.342

surface were also investigated. The calculated adsorption configurations and energies are shown in Fig. 5 and Table 2. Viewed from Table 2, fluorine atom preferentially adsorbs on the Al top site of Al_2O_3 (0001) surface with the lowest adsorption energy of −5.341 eV, followed by Mg-Al bridge site of $MgAl_2O_4$ (100) surface and Mg top site of MgO (100) surface. Adsorption intensity for a single fluorine follow this order: Al_2O_3 (0001) > $MgAl_2O_4$ (100) > MgO (100). Moreover, by comparing the adsorption energies (−1.99 to −2.03 eV) of hydrogen fluoride molecule adsorption on the α-Al_2O_3 (0001) surface [26], our calculated adsorption intensity for fluorine atom adsorption on the Al top site of Al_2O_3 (0001) surface is larger than it, indicating α-Al_2O_3 (0001) surface is more inclined to absorb fluoride atoms or ions rather than hydrogen fluoride molecules. Therefore, it is more efficiency for the beforehand treatment of dissolving hydrogen fluoride gas to the aqueous system for Al_2O_3 adsorption.

The partial density of states (PDOS) of surface atoms were investigated to provide further insight into the binding mechanism for fluorine adsorption on $MgAl_2O_4$ (100) surface, as shown in Fig. 6a. For comparison, the PDOS of clean $MgAl_2O_4$ (100) surface atoms were also studied. From Fig. 6a, adatoms fluorine atoms significantly influence the electron states of surface atom. After adsorption, *s* and *p* orbitals of Mg, Al and O atoms all shift to blue and lower in energy. Meanwhile, 2*p* orbitals of F atom are strongly hybridized with 3*s*- and 3*p*-orbitals of Al atom at the range of −6–0 eV, indicating the covalent bond characteristics for Al-F. However, electron states for *s* and *p* orbitals of Mg atom below the Fermi level are scarce, which means that electrons in the *s* and *p* orbitals of Mg atoms are almost lost. This is consistent with above analysis of Hirshfeld charges for Mg and Al absorbed with F atom. Therefore, we can conclude that the interaction between Mg and F atom is ionic. The strong orbital hybridization between Al and F atom stabilizes the F atom adsorption on $MgAl_2O_4$ (100) surface, leading to the strong interaction between F and $MgAl_2O_4$ surface.

3.3. *Fluorine adsorption on nitrogen doped $MgAl_2O_4$ (100) surface*

To further excavate the fluorine adsorption ability for $MgAl_2O_4$, nitrogen doping has been also studied. According to the reported spinel structure of MgAlON [44,45], it has the similar crystal structure to $MgAl_2O_4$ (F*d*-3*m*), in which N atoms replace a part of O atom sites in $MgAl_2O_4$ cell. Therefore, to study the effects of nitrogen doping on $MgAl_2O_4$ surface adsorption, we only considered a case of N atoms replacing two O sites on the outmost layer of $MgAl_2O_4$ (100) surface terminated with Mg atoms. Before performing adsorption calculations, the thermodynamic feasibility for this case of nitrogen doping was firstly analyzed. Calculated results indicate nitrogen doping process is feasible with a positive formation energy of 7.3 eV (704.7 kJ/mol). It is also worth pointing out that energy calculation in DFT at 0 K excludes the part of thermal vibration. Usually, the high temperature and high pressure are the key factors for the synthetic process of ceramic material. For $MgAl_2O_4$ and MgAlON, their sintering temperatures are all more than 1000 K. Combined with the experimental fact of MgAlON synthesis [44,45], we sure that the case of nitrogen doping $MgAl_2O_4$ under the high temperature condition is feasible.

On the basis of above analysis of fluorine atom preferentially adsorbing on the Mg-Al bridge site of $MgAl_2O_4$ (100) surface, so a single adatom F was initially put above the Mg-Al bridge site of nitrogen doped $MgAl_2O_4$ (100) surface and then full optimizations of its fractional coordinates for the absorption system were carried out. The calculated stable configurations of fluorine adsorption on nitrogen doped $MgAl_2O_4$ (100) surface are depicted in Fig. 5c, and the corresponding adsorption energies and geometric structure parameters are listed in Table 2. Compared to fluorine adsorption on pure $MgAl_2O_4$ (100) surface (Fig. 4c), the distortion degree of out-layer for fluorine adsorption on nitrogen doped $MgAl_2O_4$ (100) is obviously slight than it, indicating nitrogen doping can significantly enhance the stability of surface structure for $MgAl_2O_4$. The adsorption energy is −5.592 eV, which is lower than −5.341 eV of fluorine adsorption on Al_2O_3 (0001) and −5.016 eV of fluorine adsorption on the Mg-Al bridge sites of pure $MgAl_2O_4$ (100) surface. This demonstrates a fact that nitrogen doped $MgAl_2O_4$ has a more excellent fluorine adsorption ability than pure $MgAl_2O_4$, MgO and Al_2O_3.

To understand thoroughly the binding mechanism for fluorine adsorption on $MgAl_2O_4$ (100) surface, Hirshfeld charges and partial density of states (PDOS) of the surface atoms were also investigated, as shown Table 2 and Fig. 6. Seen from Table 2, more electrons transfer from the Mg-Al bridge (case F) than the case C to fluorine atom, indicating that fluorine atom adsorbs on nitrogen doped $MgAl_2O_4$ (100) surface with the stronger electrostatic interactions. Therefore, F atom more preferentially adsorbs on the Mg-Al bridge sites of nitrogen doped $MgAl_2O_4$ (100) surface, which is in agreement with the above analysis of adsorption energy. From PDOS, we can observe that the introduced N 2*p*-orbitals are strongly hybridized with 3*s*- and 3*p*-orbitals of Mg below the Fermi level. In addition, *s* and *p* orbitals of surface Mg atoms all shift to red, which is different from that case of pure $MgAl_2O_4$. After fluorine adsorption, the change rule of PDOS is approximately similar to that fluorine adsorption on pure $MgAl_2O_4$. It's also worth pointing out that the shift amplitude for *s* and *p* state of Al and O is not more obvious than the case of pure $MgAl_2O_4$. This reflects that the introduced N atom can promote electron compensation for outmost layer Al atoms after fluorine adsorption, which is also demonstrated by the results of Hirshfeld charge for N atom dramatically changing from −0.475 *e* (before adsorption) to −0.336*e* (after adsorption) and O atom indistinctively changing from −0.35 *e* (before adsorption) to −0.32 *e* (after adsorption). Therefore, we can conclude that the electron compensation effect of nitrogen atom is an important factor for enhancing the fluorine adsorption ability of nitrogen doped $MgAl_2O_4$.

4. Summary

In this work, first-principles calculations based on the density functional theory (DFT) were carried out to pore the nature of fluorine adsorption on pure and nitrogen doped $MgAl_2O_4$ surface. Surface energy analysis indicates that the low-index $MgAl_2O_4$ (100) surface terminated with Al(O) or Mg atom is the most stable and dominant surface. Moreover, $MgAl_2O_4$ surface is fluorine-loving, not hydrophilic. Compared to MgO, Al_2O_3 and $MgAl_2O_4$, the nitrogen doped $MgAl_2O_4$ (100) surface shows the outstanding fluorine adsorption performance. F atom preferentially adsorbs on the Mg-Al bridge sites of nitrogen doped $MgAl_2O_4$ (100) surface. The order of fluorine adsorption intensity is: nitrogen doped $MgAl_2O_4$ (100) > Al_2O_3 (0001) > $MgAl_2O_4$ (100) > MgO(100). In-depth PDOS analysis suggested that 2*p* orbitals of F atom strongly hybridized with 3*s*- and 3*p*-orbitals of Al atom contribute to its high adsorption strength. Furthermore, according to the analysis of Hirshfeld charge, the excellent fluorine adsorption ability of nitrogen doped $MgAl_2O_4$ attributes to the electron compensation effect of nitrogen atom and strong electrostatic interactions. Our study has identified nitrogen doped $MgAl_2O_4$ as a suitable candidate for fluorine removal in the aqueous system.

Acknowledgements

We sincerely acknowledge the High Performance Computing Center of CSU, China. This work was financially supported by the

National Science and Technology Support Project of China (No. 2012BAE08B02) and National Natural Science Foundation of China (No.51264011).

References

[1] J. Jiménez-Becerril, M. Solache-Ríos, I. García-Sosa, Fluoride removal from aqueous solutions by boehmite, Water Air Soil Pollut. 223 (2011) 1073–1078.
[2] L.A. Ramírez-Llamas, R. Leyva-Ramos, A. Jacobo-Azuara, J.M. Martínez-Rosales, E.D. Isaacs-Paez, Adsorption of fluoride from aqueous solution on calcined and uncalcined layered double hydroxide, Adsorpt. Sci. Technol. 33 (2015) 393–410.
[3] M. Nazari, R. Halladj, Optimization of fluoride adsorption onto a sonochemically synthesized nano-MgO/γ-Al_2O_3composite adsorbent through applying the L16Taguchi orthogonal design, Desalin. Water Treat. 56 (2014) 2464–2476.
[4] A. López Valdiviesoa, J.L. Reyes Bahenaa, S. Songa, R. Herrera Urbina, Temperature effect on the zeta potential and fluoride adsorption at the alpha-Al_2O_3/aqueous solution interface, J. Colloid Interface Sci. 298 (2006) 1–5.
[5] A. Mahapatra, B.G. Mishra, G. Hota, Studies on electrospun alumina nanofibers for the removal of chromium(VI) and fluoride toxic ions from an aqueous system, Ind. Eng. Chem. Res. 52 (2013) 1554–1561.
[6] J.L. Reyes Bahena, A. Robledo Cabrera, A. López Valdivieso, R. Herrera Urbina, Fluoride adsorption onto α-Al_2O_3 and its effect on the zeta potential at the alumina–aqueous electrolyte interface, Sep. Sci. Technol. 37 (2002) 1973–1987.
[7] T.-K. Oh, B. Choi, Y. Shinogi, J. Chikushi, Effect of pH conditions on actual and apparent fluoride adsorption by biochar in aqueous phase, Water Air Soil Pollut. 223 (2012) 3729–3738.
[8] Mona M. Naim, Abeer A. Moneer, Ghada F. El-Said, Defluoridation of commercial and analar sodium fluoride solutions without using additives by batch electrocoagulation–flotation technique, Desalin. Water Treat. 44 (2012) 110–117.
[9] N. Drouiche, H. Lounici, M. Drouiche, N. Mameri, N. Ghaffour, Removal of fluoride from photovoltaic wastewater by electrocoagulation and products characteristics, Desalin. Water Treat. 7 (2009) 236–241.
[10] M. Mohapatra, T. Padhia, S. Anand, B.K. Mishra, CTAB mediated Mg-doped nano Fe_2O_3: synthesis, characterization, and fluoride adsorption behavior, Desalin. Water Treat. 50 (2012) 376–386.
[11] A. Bhatnagar, E. Kumar, M. Sillanpää, Fluoride removal from water by adsorption: a review, Chem. Eng. J. 171 (2011) 811–840.
[12] S. Meenakshi, N. Viswanathan, Identifying of selective ion-exchange resin for fluoride sorption, J. Colloids Interface Sci. 307 (2007) 438–450.
[13] E. Alkan, E. Kır, L. Oksuz, Plasma modification of the anionexchange membrane and its influence on fluoride removal from water, Sep. Purif. Technol. 61 (2008) 455–460.
[14] N. Drouiche, S. Aoudj, H. Lounici, H. Mahmoudi, N. Ghaffour, M.F.A. Goosen, Development of an empirical model for fluoride removal from photovoltaic wastewater by electrocoagulation process, Desalin. Water Treat. 29 (2011) 96–102.
[15] A. Goswami, Mihir K. Purkait, The defluoridation of water by acidic alumina, Chem. Eng. Res. Des. 90 (2012) 2316–2324.
[16] S. Ghorai, K.K. Pant, Equilibrium, kinetics and breakthrough studies for adsorption of fluoride on activated alumina, Sep. Purif. Technol. 42 (2005) 265–271.
[17] S.M. Maliyekkal, S. Shukla, L. Philip, I.M. Nambi, Enhanced fluoride removal from drinking water by magnesia-amended activated alumina granules, Chem. Eng. J. 140 (2008) 183–192.
[18] X. Wu, Y. Zhang, X. Dou, M. Yang, Fluoride removal performance of a novel Fe–Al–Ce trimetal oxide adsorbent, Chemosphere 69 (2007) 1758–1764.
[19] T. Zhang, Q. Li, H. Xiao, H. Lu, Y. Zhou, Synthesis of Li–Al layered double hydroxides (LDHs) for efficient fluoride removal, Ind. Eng. Chem. Res. 51 (2012) 11490–11498.
[20] M. Mohapatra, D. Hariprasad, L. Mohapatra, S. Anand, B.K. Mishra, Mg-doped nano ferrihydrite—a new adsorbent for fluoride removal from aqueous solutions, Appl. Surf. Sci. 258 (2012) 4228–4236.
[21] D. Thakre, S. Rayalu, R. Kawade, S. Meshram, J. Subrt, N. Labhsetwar, Magnesium incorporated bentonite clay for defluoridation of drinking water, J. Hazard. Mater. 180 (2010) 122–130.
[22] P. Zhu, H. Wang, B. Sun, P. Deng, S. Hou, Y. Yu, Adsorption of fluoride from aqueous solution by magnesia-amended silicon dioxide granules, J. Chem. Technol. Biotechnol. 84 (2009) 1449–1455.
[23] C. Fang, S.C. Parker, G. de With, Atomistic simulation of the surface energy of spinel $MgAl_2O_4$, J. Am. Ceram. Soc. 83 (2000) 2082–2084.
[24] C. Fang, G. de With, Computer simulation of dissociative adsorption of water on the surfaces of spinel $MgAl_2O_4$, J. Am. Ceram. Soc. 84 (2001) 1553–1558.
[25] X. Li, Q. Hui, D.-Y. Shao, J.-J. Chen, C.-M. Li, N.-P. Cheng, Stability and electronic structure of $MgAl_2O_4$ (111) surfaces: a first-principles study, Comput. Mater. Sci. 112 (2016) 8–17.
[26] J.L. Quan, B.T. Teng, X.D. Wen, Y. Zhao, R. Liu, M.F. Luo, Hydrogen fluoride adsorption and reaction on the alpha-Al_2O_3 (0001) surface: a density functional theory study, J. Chem. Phys. 136 (2012) 114701.
[27] X. Li, J. Paier, Adsorption of water on the Fe_3O_4 (111) surface: structures, stabilities, and vibrational properties studied by density functional theory, J. Phys. Chem. C 120 (2016) 1056–1065.
[28] M. Ruan, H. Hou, W. Li, B. Wang, Theoretical study of the adsorption/dissociation reactions of formic acid on the α-Al_2O_3 (0001) surface, J. Phys. Chem. C 118 (2014) 20889–20898.
[29] H. Hu, L. Reven, A.D. Rey, DFT study of gold surfaces–ligand interactions: alkanethiols versus halides, J. Phys. Chem. C 119 (2015) 11909–11913.
[30] A. Kokalj, S. Peljhan, Density functional theory study of adsorption of benzotriazole on Cu_2O surfaces, J. Phys. Chem. C 119 (2015) 11625–11635.
[31] J. Zhao, M.-C. He, Theoretical study of heavy metal Cd, Cu Hg, and Ni(II) adsorption on the kaolinite (001) surface, Appl. Surf. Sci. 317 (2014) 718–723.
[32] S. Jungsuttiwong, Y. Wongnongwa, S. Namuangruk, N. Kungwan, V. Promarak, M. Kunaseth, Density functional theory study of elemental mercury adsorption on boron doped graphene surface decorated by transition metals, Appl. Surf. Sci. 362 (2016) 140–145.
[33] John P. Perdew, K. Burke, M. Ernzerhof, Generalized gradient approximation made simple, Phys. Rev. Lett. 77 (1996) 3865–3868.
[34] G. Kresse, Efficient iterative schemes for ab initio total-energy calculations using a plane-wave basis set, Phys. Rev. B 54 (1996) 169–186.
[35] K. Laasonen, R. Car, C. Lee, D. Vanderbilt, Implementation of ultrasoft pseudo potentials in ab initio molecular dynamics, Phys. Rev. B 43 (1991) 6796.
[36] H.J. Monkhorst, J.D. Pack, Special points for Brillouin-zone integrations, Phys. Rev. B 13 (1976) 5188.
[37] Y. Li, B. Huang, X. Cheng, Y. Zhang, Achieving high specific capacity through a two-electron reaction in hypothetical Li_2VFSiO_4: a first-principles investigation, J. Electrochem. Soc. 162 (2015) A787–A792.
[38] C.J. O'Brien, Z. Rák, D.W. Brenner, Calculated stability and structure of nickel ferrite crystal surfaces in hydrothermal environments, J. Phys. Chem. C 118 (2014) 5414–5423.
[39] J.L. Nie, H.Y. Xiao, F. Gao, X.T. Zu, Electronic and magnetic properties of Al adsorption on α-uranium (001) surface: Ab initio calculations, J. Alloys Compd. 476 (2009) 675–682.
[40] R. Khenata, M. Sahnoun, H. Baltache, M. Rérat, A.H. Reshak, Y. Al-Douri, B. Bouhafs, Full-potential calculations of structural, elastic and electronic properties of $MgAl_2O_4$ and $ZnAl_2O_4$ compounds, Phys. Lett. A 344 (2005) 271–279.
[41] N.J. Van Der Laag, C.M. Fang, G. De With, G.A. De Wijs, H.H. Brongersma, Geometry of {001} surfaces of spinel ($MgAl_2O_4$): first-principles simulations and experimental measurements, J. Am. Ceram. Soc. 88 (2005) 1544–1548.
[42] X. Ouyang, M. Lei, S. Shi, C. Luo, D. Liu, D. Jiang, Z. Ye, M. Lei, First-principles studies on surface electronic structure and stability of $LiFePO_4$, J. Alloys Compd. 476 (2009) 462–465.
[43] P. Zhang, D. Zhang, L. Huang, Q. Wei, M. Lin, X. Ren, First-principles study on the electronic structure of a $LiFePO_4$ (010) surface adsorbed with carbon, J. Alloys Compd. 540 (2012) 121–126.
[44] X. Liu, H. Wang, B. Tu, W. Wang, Z. Fu, Novel divalent europium doped MgAlON transparent ceramic for shortwave ultraviolet erasable windows, Scripta Mater. 105 (2015) 30–33.
[45] G. Ye, J. Shang, D. Zhang, M. Liang, Y. Chen, Synthesis and oxidation behavior of MgAlON prepared from different starting materials, J. Am. Ceram. Soc. 93 (2009) 322–325.